



International Conference on
**RESEARCHES
IN SCIENCE &
ENGINEERING**

CERTIFICATE

Istanbul University- TURKEY
July 2016

Verification Code : **AE-CDBE**
System Address www.icrsie.com/verify

Certificate of Participating in Educational Course

Dear Mr. / Ms. Ali Kianifar

Hereby this is to certify that you have participated in international Conference on Researches in Science & Engineering held on 28 July, 2016 at Istanbul University for 16 hours. We ask the almighty your ever-increasing success in knowledge and research areas.

Sincerely
Eng. Ahmet Imadi
Conference Chair



An analytical study on energy and exergy of a minichannel-based solar collector using Fe_3O_4 and MgO /water nanofluids

Moeen Amini^{1*}, Ali Kianifar¹

1. Department of Mechanical Engineering, Ferdowsi University of Mashhad, Mashhad, Iran, a-kiani@um.ac.ir

Abstract

Flat plate solar collector (FPSC) is one of the essential solar devices that can be utilized for heating purposes in either residential or civil buildings. Its mechanism is simple: solar radiation that passes through one or more transparent glasses received by the risers' surfaces and absorber plate of a FPSC. Concomitant of this period, operating fluid acquires sufficient time to absorb the energy stored in the risers and absorber of the FPSC. As a result, outlet temperature of the operating fluid flows within risers augments. However, in this paper, to conduct a mathematical investigation, a MATLAB code has been developed to illuminate the effect of using two different nanoparticles namely Fe_3O_4 and MgO suspended within pure base water of a flat plate solar collector (FPSC) from energy and exergy points of view. Results are being presented for two different mass flow rates, and comparisons are being established for various consequential parameters. Considering the attained outcomes, it is found that using Fe_3O_4 /water nanofluids provides higher thermal efficiency and entropy generation rate value, whereas exploitation of MgO /water nanofluids creates the lowest thermal efficiency and entropy generation rate value. Moreover, the highest outlet temperature obtains when Fe_3O_4 /water nanofluids are used.

Key words: Minichannel solar collector, Entropy generation, Nanofluids, Heat transfer

1. Introduction

Due to detrimental interdependent of fossil fuels exploitations in human life, it is a great and logical idea to fabricate systems that generate desired yields using renewable energy sources namely solar, biomass, tides and eventually winds [1]. However, solar energy shows a promising future since it is abundant, free and almost available in almost every part of the world. Amongst great deals of solar devices, flat plate solar collectors (FPSC) are popular and can be utilized for heating purposes in residential, commercial and civil buildings. Researchers have been striving to develop FPSCs that are much more

efficient. One of the applicable solutions that would increase the outlet temperature of conventional FPSCs and simultaneously would augment thermal performance of these facilities is to add different nanoparticles within the base fluid with the size of 1-100 nm [2]. Khullar et al. [3] studied the effect of applying Al/Therminol VP-1 nanofluids on the performance of a concentrating parabolic solar collector (CPSC). Their results revealed that nanofluids based CPSC have higher efficiency by about 10%, in comparison with conventional CPSC. Tyagi et al. [4] established a theoretical investigation of the potential of Alumina/water nanofluids to alleviate the efficiency of non-concentrating direct absorption solar collector. They concluded that the performance of their system improves by around 10%, compared to that of the common one. Colangelo et al. [5] fabricated a new FPSC to solve the problem of sedimentation of nanofluids in the solar collector. Additionally, they added Al_2O_3 /water nanofluids to appraise the increment taken place in thermal efficiency of their system. They mentioned that the heat transfer coefficient rocketed by around 25%.

Parvin et.al [6] conducted an analysis to evaluate heat transfer and entropy generation due to the utilization of Cu/water and Ag/water nanofluids in a direct absorption solar collector. Their results demonstrated that higher volume fraction of nanoparticles leads to increasing both Reynolds number (Re) and entropy generation. Moreover, they propounded a correlation for Nusselt number for the condition that Re and volume fraction are less than 10^3 and 3%, respectively. Mahian et al. [7] studied the effect of pH and nanoparticles' diameter in entropy generation rate of a flat plate solar collector when SiO_2 /water nanofluids are employed. They found that for nanofluids containing the particles with the size of 16 nm, the increase in the pH increases the entropy generation, while inverse results obtain when nanofluids with 12 nm particles size are exploited. What is more, Mahian et al. [8, 9] reviewed entropy generation due to nanofluids in a multiplicity of thermal systems.

The pivotal purpose of this present work is to find out utilization of which nanofluids is efficient from first and second laws of Thermodynamics. The effect of the pressure drop within the risers of the solar collector has also taken into account of this study.

1.Problem description:

In this research paper, the under-investigated problem is a minichannel-based solar collector demonstrated in Fig.1. The specifications of the FPSC are tabulated in Table 1. It is assumed that the risers of the FPSC are parallel, and the centerlines of the absorber plate and risers are situated on the same line.

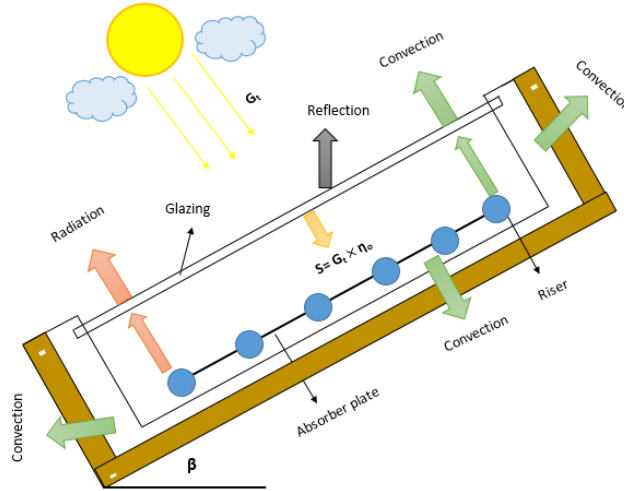


Fig. 1. Schematic diagram of the FPSC with risers in which straight-shaped fins are installed.

Table 1. Specifications for the under-investigated FPSC

Collector parameters	
Relative roughness of risers (ε/D_i)	0.04296
Collector slope, β	36°
Plate thickness, δ_c	1.5 mm
Optical efficiency, η_0	0.85
Tube spacing, W	15 cm
Number of risers	15
Length of collector, L	3 m
Inner diameter of pipes, D_i	2 mm
Outer diameter of pipes, D_o	2.5 mm
Thickness of back insulation, t_b	2 cm
Thickness of edge insulation, t_e	1 cm
Emissivity of absorber plate, ε_p	0.92
Emissivity of glass cover, ε_g	0.88
Thermal conductivity of back insulation, k_b	4 W/cm K
Thermal conductivity of edge insulation, k_e	4 W/cm K
Thermal conductivity of plate, k_c	40 W/m K

To evaluate the performance of the FPSC, real meteorological data was attained from the meteorological station center in Mashhad, Iran for a typical day in summer at 2:00 pm. The meteorological data was depicted in Table 2.

Table 2. Meteorological data for 2:00 p.m. in a typical day in summer for Mashhad, Iran

Time	Solar irradiance (W/m^2)	Ambient Temperature (K)	Wind velocity (m/s)
2:00 PM	815	308	1.25

Pure water, different nanoparticles listed in Table 3 and two constant mass flow rate, 0.25 and 0.75 kg/s, are considered in the present work. The physical properties of nanoparticles and water at 300 K are provided in Table 3.

Table 3. Thermo physical properties of water and nanoparticles			
	K (W/m K)	C_p (J/kg K)	ρ (kg/m ³)
Water	0.613	4180	998
Fe ₃ O ₄	6.0	670	5200
MgO	45	955	3560

3. Mathematical Formulation:

Prior to present mathematical modeling of the minichannel solar collector, several assumptions must be mentioned:

- Risers are parallel, and the centerlines of absorber plate and the risers are situated in the same line.
- The flow in the solar collector is fully developed and steady.
- Uniform fluid is flowing within the risers.
- Negligible temperature gradients in the radial direction.

The nanoparticles are well dispersed in the pure water to form a homogeneous mixture.

3.1 Nanofluid Properties:

Density and heat capacity of the nanofluids can be acquired using the following equations[10]:

$$\rho_{nf} = \rho_f(1-\phi) + \rho_p\phi \quad (1)$$

$$C_{p,nf} = \frac{\rho_f C_{p,f}(1-\phi) + \rho_p C_{p,p}\phi}{\rho_{nf}} \quad (2)$$

Where ρ , ϕ , C_p are density (kg/m³), the volume fraction of nanoparticles and heat capacity (J/kg K), respectively. The subscripts of nf, f, and p illustrate for nanofluid, base fluid and nanoparticle, respectively.

The thermal conductivity of nanofluids is estimated by Xuan et al. [11] model that was posed with respect to the aggregation and Brownian motion of nanoparticles. The model can be defined as:

$$\frac{K_{nf}}{K_f} = \frac{K_p + 2K_f - 2\phi(K_f - K_p)}{K_p + 2K_f + \phi(K_f - K_p)} + \frac{\rho_p\phi C_{p,f}}{2K_f} \sqrt{\frac{2k_B T_{ave}}{3\pi d_p \mu_f}} \quad (3)$$

Where K , K_B , d_p , T_{ave} and μ are thermal conductivity (W/m K), Boltzmann constant (m²kg/s² K), particle size (m), average temperature (K) and eventually viscosity (kg/m s), respectively. The thermal conductivity of the base fluid (water) can be assessed from the following correlation [12]:

$$K_f = 0.6067 \left(1.26523 + 3.704 \left(\frac{T_{ave}}{298.15} \right) - 1.43955 \left(\frac{T_{ave}}{298.15} \right)^2 \right) \quad (4)$$

The average temperature for calculation the above-mentioned equations are defined as below:

$$T_{ave} = \frac{T_{in} - T_{out}}{\ln \left(\frac{T_{in}}{T_{out}} \right)} \quad (5)$$

The viscosity of the base fluid is determined by correlation presented by Corcione [13] that is valid for volume fraction up to 10% and nanoparticle sizes larger than 25 nm:

$$\mu_{nf} = \frac{\mu_f}{1 - 34.87 \left(\frac{d_p}{d_f} \right)^{-0.3} \phi^{1.03}} \quad (6)$$

Where d_f is the molecular diameter of the base fluid:

$$d_f = 0.1 \left(\frac{6M}{N\pi\rho_{f0}} \right)^{\frac{1}{3}} \quad (7)$$

In which M, N and ρ_{f0} are the molecular weight of the base fluid, Avogadro number, and base fluid density at 293 (K), respectively.

The viscosity of base fluid can be attained by:

$$\mu_f = 2.414 \times 10^{-5} \times 10^{\frac{247.8}{(T_{ave} - 140)}} \quad (8)$$

3.2 First law of Thermodynamics analysis:

Solar radiation with the intensity of G_t is received by the glass cover of the FPSC. The predominant part of which, i.e. $S = \eta_0 \times G_t$ strikes to the absorber plate of the FPSC. The amount of solar radiation absorbed by the operating fluid is defined by Q_u , and the remained part is dissipated through the edges, bottom and top of the absorber plate to the surrounding. To evaluate the outlet temperature and efficiency of the FPSC, an approach should be established to appraise the heat losses occurred to the surroundings initially. The relation governed between the absorbed heat and heat losses are as follows:

$$Q_u = A_c [S - U_L (T_p - T_a)] \quad (9)$$

Where A_c , S , U_L , T_p and T_a are collector surface area (m^2), the amount of solar radiation received by the absorber plate (W/m^2), overall heat loss coefficient of the FPSC ($W/m^2 K$), plate and ambient temperatures (K), respectively.

Assuming that all the heat losses of the FPSC taken place to a sink temperature T_a , U_L can be defined as [14]:

$$U_L = U_t + U_b + U_e \quad (10)$$

In which U_t , U_b and U_e are heat loss coefficients from top, bottom, and edges of the FPSC, respectively. Heat loss from the top surface of the FPSC comprised of both radiation and convection phenomena and can be computed by the below correlation [15]:

$$U_t = \frac{1}{N_g} + \frac{\sigma(T_p^2 + T_a^2)(T_p + T_a)}{\frac{1}{\varepsilon_p + 0.05N_g(1 - \varepsilon_p)} + \frac{2N_g + \tau - 1}{\varepsilon_g} - N_g} \quad (11)$$

$$\frac{c}{T_p} \left[\frac{T_p - T_a}{N_g + \tau} \right]^{0.33} + \frac{1}{h_w}$$

Where N_g , σ , ε_p and ε_g are the number of glass covers, Stefan-Boltzmann constant, the emissivity of plate and glass covers that are given in Table 1. The parameter of h_w conveys the wind heat transfer coefficient and is calculated by:

$$h_w = \frac{8.6V_w^{0.6}}{L^{0.4}} \quad (12)$$

Where V_w , L are wind velocity (m/s) and collector length (m), respectively. Additionally, c and τ are constants that can be defined as [15]:

$$C = 365.9(1 - 0.00883\beta + 0.00001298\beta^2) \quad (13)$$

$$\tau = (1 - 0.04h_w + 0.0005h_w^2)(1 + 0.09N_g) \quad (14)$$

Where β is the tilt angle of the FPSC that are tabulated in Table 1. To evaluate heat losses happened from bottom and edges of the FPSC, following equations should be exploited:

$$U_b = \frac{1}{\frac{t_b}{K_b} + \frac{1}{h_{b,a}}} \quad (15)$$

$$U_e = \frac{1}{\frac{t_e}{K_e} + \frac{1}{h_{e,a}}} \frac{A_e}{A_c} \quad (16)$$

In which K_b , K_e , t_e , t_b , $h_{b,a}$, $h_{e,a}$, A_e are bottom and edges thermal conductivities of insulators, thicknesses of bottom and edges insulators, convection heat transfer coefficients ($W/m^2 K$) and surface area of the FPSC's edges, respectively.

For computing overall and top heat loss coefficients of the FPSC, the value of T_p should be determined. However, to satisfy this purpose, an initial logical guess is predicted. Therefore, the quantities of both heat loss coefficients and Q_u are determined. In the next stage, the value of T_p is calculated by the following relation and the initial guess is rectified through an iterative approach:

$$T_p = T_{in} + \frac{Q_u}{A_c F_R U_L} (1 - F_R) \quad (17)$$

The error criterion used for the iterative process is employed by:

$$\left| \frac{(T_p)_{guess} - (T_p)_{calculated}}{(T_p)_{calculated}} \right| \leq 10^{-5} \quad (18)$$

Heat removal coefficient, F_R , is defined as [15]:

$$F_R = \frac{\dot{m} C_p}{A_c U_L} \left[1 - \exp \left(- \frac{U_L F' A_c}{\dot{m} C_p} \right) \right] \quad (19)$$

In the prior relation, F' is the efficiency factor of the collector as [15]:

$$F' = \frac{\frac{1}{U_L}}{W \left[\frac{1}{U_L [D + (W - D) F]} + \frac{1}{\pi D_i h_{fi}} \right]} \quad (20)$$

Where W , D , D_i and F are tube spacing (m), the outer and inner diameter of risers (m) and finally standard fin efficiency, respectively.

The standard fin efficiency is obtained using following equations:

$$F = \frac{\tanh [m(W - D) / 2]}{m(W - D) / 2} \quad (21)$$

Where

$$m = \sqrt{\frac{U_L}{K_c \delta_c}} \quad (22)$$

In which K_c and δ_c are thermal conductivity and thickness of the absorber plate tabulated in Table 1, respectively.

Attaining internal heat transfer coefficient (h_{fi}), below definition of the Nusselt number should be employed:

$$h_{fi} = \frac{Nu K_n f}{D_i} \quad (23)$$

For calculation of the Nusselt number, Gnielinski [16] propounded a correlation that is applicable for $3 \times 10^3 \leq Re \leq 5 \times 10^5$ and $0.5 \leq Pr \leq 2000$, and also is applicable for the conditions that nanoparticles are mixed within the pure base fluid [7]:

$$Nu = \frac{(f/8)(Re-1000)Pr}{1 + 12.7(f/8)^{1/2} \left(\frac{2}{Pr^3 - 1} \right)} \quad (24)$$

Where f , Re and Pr are friction factor, Reynolds and Prandtl numbers, respectively. To assess the value of the friction factor for turbulent flows, Colebrook correlation must be solved [17]:

$$\frac{1}{\sqrt{f}} = -2 \log \left(\frac{\varepsilon}{D_i} + \frac{2.51}{Re \sqrt{f}} \right) \quad (25)$$

Reynolds and Prandtl numbers are described as:

$$Re = \frac{4\dot{m}_r}{\pi D_i \mu_{nf}} \quad (26)$$

$$Pr = \frac{\mu_{nf} C_{p,nf}}{K_{nf}} \quad (27)$$

The aforementioned time consumption computations should be undertaken to accomplish the mean temperature of the absorber plate, T_p .

Eventually, the outlet temperature of the nanofluid can be attained as follows: $T_{out} = T_{in} + \frac{Q_u}{\dot{m} C_p}$ (28)

Thermal efficiency of the FPSC can be obtained as [7]:

$$Efficiency(\%) = \frac{Q_u}{A_c G_t} \times 100 \quad (29)$$

3.3 Pressure drop:

To calculate the pressure drop, first the major and minor head losses should be calculated. Major head loss is produced due to the flow of fluid in pipes while the minor head loss is created due to fittings, entering and exiting of fluid, and so on. The major head loss in a solar collector having n parallel risers is obtained by [18]:

$$h_{l,major} = h_{l,riser 1} = h_{l,riser 2} = \dots = h_{l,riser n} \quad (30)$$

The total head loss (h_l) is the sum of major head loss and minor head loss and its value is equal to:

$$h_L = h_{l,major} + h_{l,min or} = \frac{8\dot{m}_r^2}{\rho^2 g \pi^2 D_i^4} \left(f \frac{L_r}{D_i} + \sum K_L \right) \quad (31)$$

Where K_L , L_r are loss coefficient and length of the riser, respectively. Assuming a sharp-edged connection between the headers and risers, the values of K_L for entering and exiting the fluid are 0.5 and 1, respectively [18].

Considering the Bernoulli relation between the inlet and outlet of the risers, the pressure drop is determined:

$$\frac{P_1}{\rho g} + z_1 = \frac{P_2}{\rho g} + z_2 + h_L \quad (32)$$

Simplifying Eq. 32, it can be defined as below:

$$\Delta P = P_1 - P_2 = \rho g (L \sin \beta + h_L) \quad (33)$$

Where

$$L_r \sin(\beta) = (Z_2 - Z_1) \quad (34)$$

$Z_2 - Z_1$ is the vertical distance between the outlet and inlet of the riser.

3.4 Second law of Thermodynamics analysis:

In this present study, calculation of the lost work has been presented to find out the total entropy generation, \dot{S}_{gen} (W/K). Lost work of the FPSC consists of both leakage (\dot{E}_l) and destroyed (\dot{E}_d) exergy rates. Relation that establishes a relation between the lost work and entropy generation is [19]:

$$\dot{S}_{gen} = \frac{\dot{E}_d + \dot{E}_l}{T_a} = \frac{\dot{W}_{lost}}{T_a} \quad (35)$$

The destroyed exergy rate composed of 3 different terms:

1. Temperature difference between sun and absorber plate
 2. Pressure drop in the FPSC
 3. Nanofluid flow in the FPSC and temperature difference between nanofluid and absorber plate
- Hence, applying the aforesaid terms, the destroyed exergy can be obtained as below:

$$\dot{E}_d = \dot{E}_{d,\Delta T_s} + \dot{E}_{d,\Delta P} + \dot{E}_{d,\Delta T_f} \quad (36)$$

Where [31-34]

$$\dot{E}_{d,\Delta T_s} = \eta_0 G_t A_c T_a \left(\frac{1}{T_p} - \frac{1}{T_s} \right) \quad (37)$$

$$\dot{E}_{d,\Delta P} = \frac{\dot{m} \Delta P}{\rho} \frac{T_a \ln \left(\frac{T_{out}}{T_a} \right)}{(T_{out} - T_{in})} \quad (38)$$

$$\dot{E}_{d,\Delta T_f} = \dot{m} C_p T_a \left(\ln \left(\frac{T_{out}}{T_a} \right) - \frac{(T_{out} - T_{in})}{T_p} \right) \quad (39)$$

The leakage exergy is:

$$\dot{E}_d = U_l A_c (T_p - T_a) \left(1 - \frac{T_a}{T_p} \right) \quad (40)$$

Therefore, by substituting Eqs. (35)–(38) in Eq. (33), the total entropy generation rate is caused by two effects, first the temperature difference and consequently heat transfer, and the second i.e. fluid friction and consequently the pressure drop, $(\dot{S}_{gen})_F$. The following relation can be used to calculate the entropy generation:

$$\dot{S}_{gen} = \underbrace{\eta_0 G_t A_c T_a \left(\frac{1}{T_p} - \frac{1}{T_s} \right) + \dot{m} C_p \left(\ln \left(\frac{T_{out}}{T_a} \right) - \frac{(T_{out} - T_{in})}{T_p} \right) + U_L A_c \left(\frac{T_p}{T_a} - 1 \right) \left(1 - \frac{T_a}{T_p} \right)}_{(\dot{S}_{gen})_H} + \underbrace{\frac{\dot{m} \Delta P}{\rho n f} \frac{\ln \left(\frac{T_{out}}{T_a} \right)}{(T_{out} - T_{in})}}_{(\dot{S}_{gen})_F} \quad (41)$$

Where η_0 , G_t , \dot{m} , ΔP , T_s , T_{in} and T_{out} are optical efficiency, solar irradiance on the FPSC (W/m^2), mass flow rate of nanofluid (kg/s), pressure drop (Pa), apparent sun temperature (K), inlet and outlet temperatures of the nanofluid (K), respectively.

4. Results and Discussions:

In this paper, a mathematical investigation has been conducted to study and compare energy and exergy efficiencies of a flat plate solar collector (FPSC) working with four different nanofluids.

Fig.2 shows the variations of the Nusselt number with different volume fractions of MgO/water and $\text{Fe}_3\text{O}_4/\text{water}$ nanofluids for two various mass flow rates, i.e. 0.25 and 0.75 kg/s. As it is pellucid, increasing in the volume fraction of both nanofluids eventuates

in abating the Nusselt number. The reason that can be addressed for such plummet can be described using Eq. (24). Creation of a mixture with more dispersed nanoparticles results in higher effective viscosity. Due to an inverse relation governed between effective viscosity and Reynold number, Reynolds number decreases and, therefore, downward trends are being seen in the Nusselt number variation. However, for all the MgO/water and Fe₃O₄/water nanofluids, it is found that Pr number is lower than pure water. Therefore, decrease in the Pr number also consolidates the plummet happened in the Nusselt number in addition to Re. Moreover, as it is expected, increasing in the mass flow rate results in having higher Re number inside the tube and, thus logically, higher Nusselt number will generate.

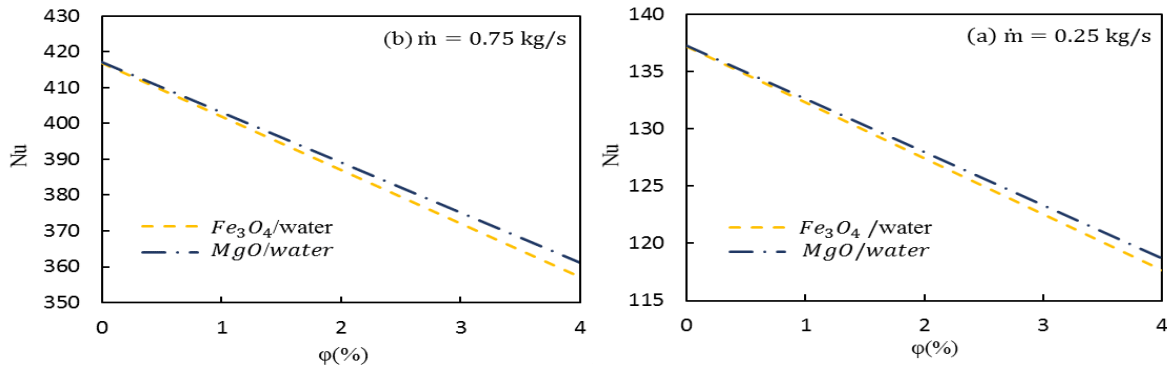


Fig. 2. Variations of Nusselt number with volume fraction for different nanofluids

(a) $\dot{m} = 0.25 \text{ kg/s}$ and (b) $\dot{m} = 0.75 \text{ kg/s}$.

Fig. 3 delineates variations of the convective heat transfer coefficient versus different volume fraction of MgO and Fe₃O₄/water nanofluids for two various mass flow rates inside the mini-channel based solar collector. Augmentation in the nanofluids volume concentration results in providing lower heat transfer rate similar to the variations of the Nusselt number discussed in Fig. 2. Increasing in the volume fraction of nanoparticles within water eventuates in creation of a mixture with higher effective thermal conductivity, referred to Eq. (3).

Therefore, based on Eq. (23), the heat transfer coefficient inside the system slumps. As it is obvious, jumping in the mass flow rate, from 0.25 to 0.75 kg/s, causes a noticeable increase in the value of heat transfer coefficient. The reason for having such substantial increase is the small hydraulic diameter of the tube. Furthermore, since mixture of MgO nanoparticles with pure water generates lower value of effective thermal conductivity with respect to the Fe₃O₄/water nanofluids, its usage is preferable from first laws of Thermodynamics.

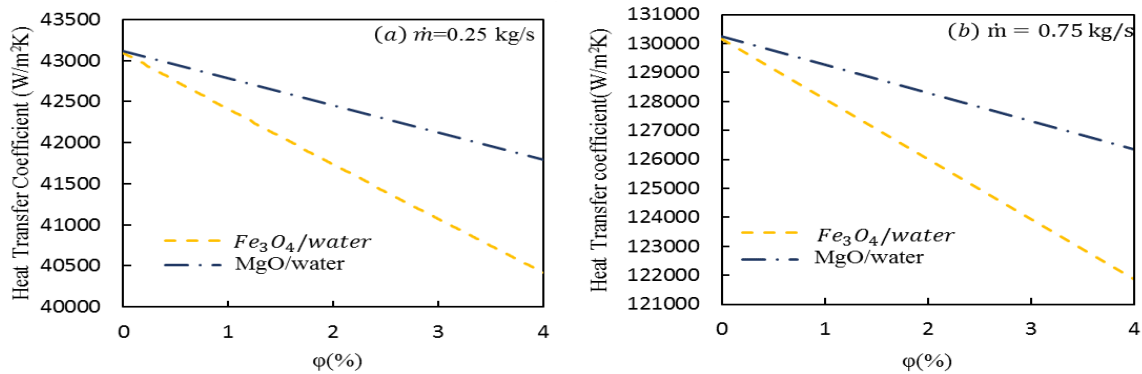


Fig.3 delineates variations of the convective heat transfer coefficient versus different volume fraction of MgO and Fe_3O_4 /water nanofluids for two various mass flow rates.

The variations of the outlet temperature with different volume fractions of nanoparticles for two different mass flow rates of 0.25 and 0.75 kg/s are plotted in Fig. 4. It is clear that Fe_3O_4 /water and MgO /water nanofluids create the highest and lowest outlet temperature, respectively.

It can be perceived that the nanofluids that provide the highest heat transfer coefficient value do not necessarily generate the highest outlet temperature whilst the Fe_3O_4 /water nanofluid that produce the lowest heat transfer coefficient generate the highest outlet temperature . Increasing the volume fraction of nanoparticles also leads to increasing in the outlet temperature. Using Eq. (28) justifies that the outlet temperature substantially relies on the effective heat capacity of nanofluids. Hence, Fe_3O_4 /water nanofluids which have the lowest effective heat capacity provide the highest outlet temperature whereas the MgO /water nanofluids which produce the highest effective heat capacity have the lowest outlet temperature. On the other hand, Fe_3O_4 /water nanofluids have the higher effective density. Having the lowest velocity makes it possible for Fe_3O_4 /water nanofluids to absorb much more thermal energy.

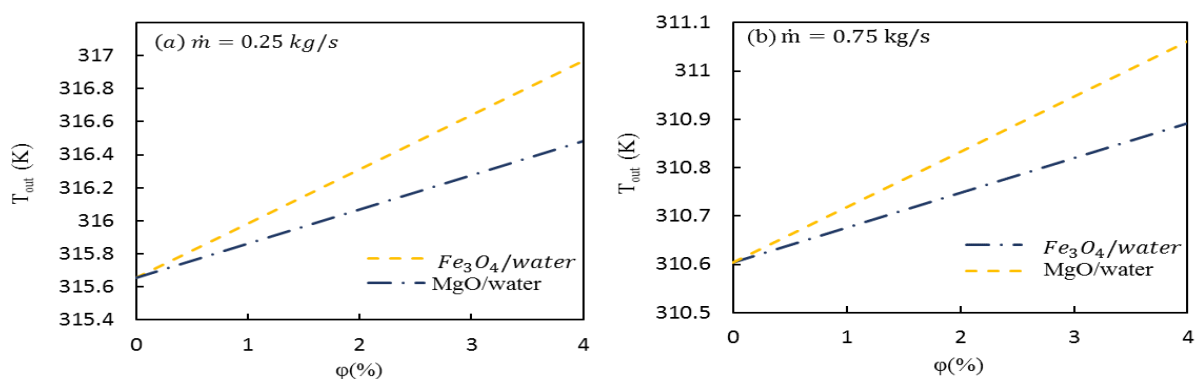


Fig. 4. Variations of outlet temperature of nanofluids versus different volume fractions of the nanoparticles (a) $\dot{m} = 0.25$ kg / s and (b) $\dot{m} = 0.75$ kg / s .

Variations of the thermal efficiency of the flat plate solar collector (FPSC) are delineated as the function of volume fraction of nanoparticles for two different mass flow rates in Fig.5. As observed, efficiency has opposite behavior compared to the outlet temperature for both of nanofluids. MgO/water nanofluids have the minimum value of

efficiency while Fe_3O_4 /water nanofluids display the highest value of efficiency. When Fe_3O_4 /water nanofluids are utilized, the mean temperature of the absorber plate will be highest and based on Eq. (9), the value of the absorbed heat is minimized. Consequently, considering thermal efficiency definition given in Eq. (29), the efficiency of the FPSC dips. However, exploitation of MgO /water nanofluids leads to having the lowest mean absorber plate's temperature and thereby higher thermal efficiency will be attained. What is more, increasing the mass flow rate of nanofluids causes a marginal augmentation in the efficiency values for all of the nanofluids in a fixed volume fraction value. When the mass flow rate of nanofluids increases, the mean temperature of the absorber plate reduces and as a result the value of the absorbed heat boosts and simultaneously thermal efficiency of the system increases.

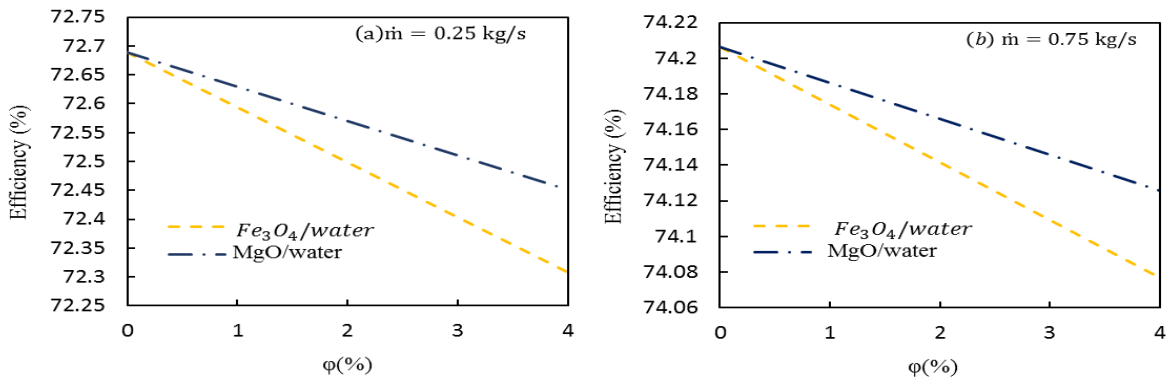


Fig. 5. Variations of thermal efficiency versus different volume fractions of the nanoparticles (a) $\dot{m} = 0.25 \text{ kg/s}$ and (b) $\dot{m} = 0.75 \text{ kg/s}$.

Fig.6 shows the variations of pressure drop with the volume fraction of four different nanofluids and two different mass flow rates. It is found that adding nanoparticles to the pure base fluid (water) leads to decreasing the pressure drop phenomenon. Also, increasing the particle loads to the water results in declining the pressure drop value much more. Utilization of Fe_3O_4 /water nanofluids generates the lowest pressure drop value whereas using MgO /water nanofluids creates the highest value of the pressure drop. The following relation governs between the pressure drop, friction factor and density of nanofluids when minor losses are neglected:

$$\Delta P \approx \frac{\dot{m}^2}{\rho_{nf}} f \quad (42)$$

Regarding the constant mass flow rate, the friction factor of nanofluids is higher, compared to that of water, but since the density of nanofluid becomes higher than pure water, the pressure drop of nanofluids will become lower than pure water. Hence, adding Fe_3O_4 & MgO can increase the effective density sufficiently and the increment created in the effective density dominates the increase happened in the friction factor of nanofluids. As a result, pressure drop lines for various aforesaid nanofluids drop. However, since the Fe_3O_4 has the highest value of density amongst different nanoparticles tabulated in Table 3 (about 5200 kg/m^3), the pressure drop pertinent to Fe_3O_4 /water nanofluids is lowest. Besides, an augmentation in the mass flow rate can increase the value of the pressure drop markedly for a fixed volume fraction of nanoparticles.

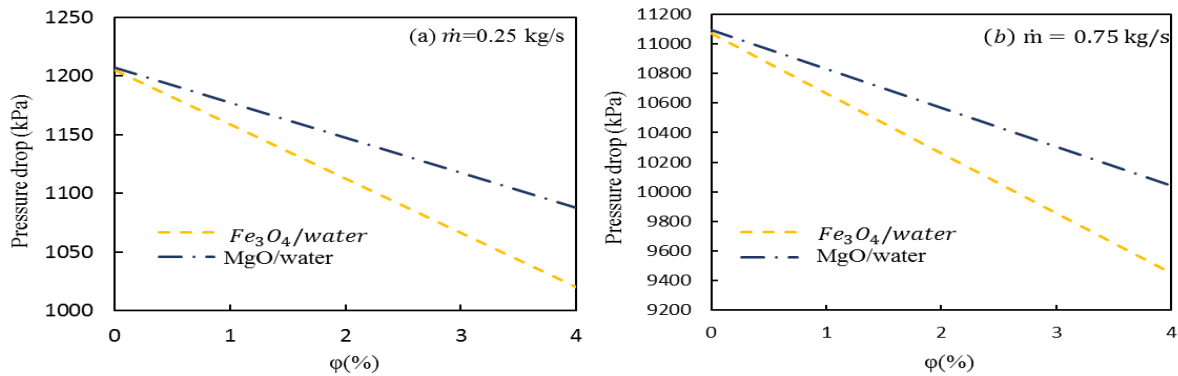


Fig. 5. Variations of pressure drop with volume fractions of the nanoparticles (a) $\dot{m} = 0.25$ kg / s and (b) $\dot{m} = 0.75$ kg / s .

Results for the entropy generation rate for nanofluids and two different mass flow rates are posed in Fig. 6. It is found that using nanofluids instead of water can reduce the entropy generation rate. To answer such alteration, Eq. (41) must be taken into account. In Eq. (41) the first and fourth terms on the right hand of the equation play the prominent role in determination of the entropy generation rate. For low mass flow rate (0.25 kg/s), the first term will become great deal essential, compared to the fourth term. This term displays that when the mean temperature of the absorber plate increases, the value of the entropy generation rate is become lower. The fourth term will be more important when the mass flow rate increases. For the mass flow rate of 0.75 kg/s, this term expresses that the entropy generation rate is directly proportional to pressure drop while has a converse relation with density. However, in reference to Fig.6 , it is expected that the entropy generation rate decreases since the pressure drop plummets. Fe_3O_4 /water nanofluids have the minimum entropy generation rate while MgO/water nanofluids have the highest rate of entropy generation.

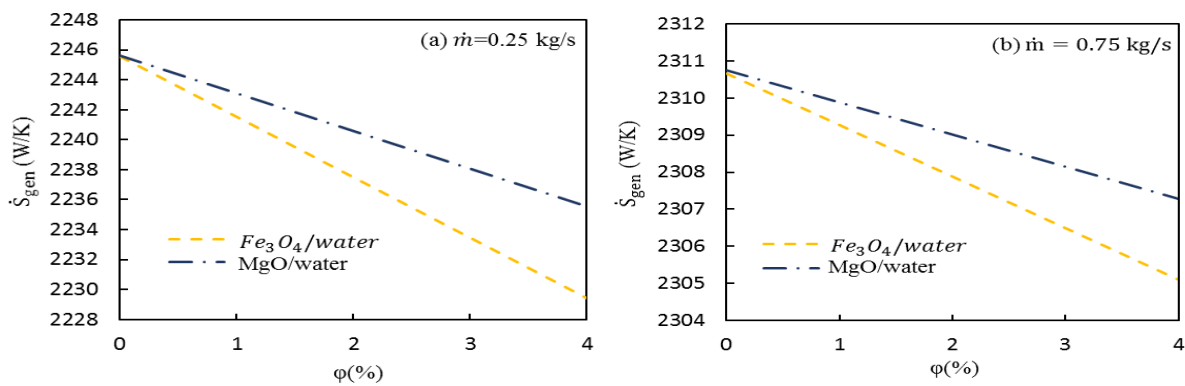


Fig. 6. Variations of entropy generation rate with volume fractions of the nanoparticles (a) $\dot{m} = 0.25$ Kg / s and (b) $\dot{m} = 0.75$ Kg / s .

Acknowledgement:

The authors gratefully acknowledge Mr. Mojtaba Edalatpour.

References

- [1] Edalatpour M, Kianifar A, Ghiami Sh, Effect of blade installation on heat transfer and fluid flow within a single slope solar still. *International Communications in Heat and Mass Transfer* 2015; 66:61-70.
- [2] Colangelo G, Favale E, de Risi A, Laforgia D. A new solution for reduced sedimentation flat panel solar thermal collector using nanofluids. *Applied Energy* 2013; 111:80–93.
- [3] Khullar V, Tyagi H, Phelan PE, Otanicar TP, Singh H, Taylor RA. Solar energy harvesting using nanofluids-based concentrating solar collector. *Journal of Nanotechnol Engineering Medicine* 2012; 3:031003.
- [4] Tyagi H, Phelan P, Prasher R. Predicted efficiency of a low-temperature nanofluid based direct absorption solar collector. *Journal of Solar Energy Engineering* 2009; 131:041004.
- [5] Colangelo G, Favale E, de Risi A, Laforgia D. A new solution for reduced sedimentation flat panel solar thermal collector using nanofluids. *Applied Energy* 2013; 111:80–93.
- [6] Parvin S, Nasrin R, Alim MA. Heat transfer and entropy generation through nanofluid filled direct absorption solar collector. *International Journal of Heat and Mass Transfer* 2014; 71:386–95.
- [7] Mahian O, Kianifar A, Sahin AZ, Wongwises S, Performance analysis of a minichannel-based solar collector using different nanofluids. *Energy Conversion and Management* 2014; 88:129-138.
- [8] Mahian O, Kianifar A, Kalogirou SA, Pop I, Wongwises S. A review of the applications of nanofluids in solar energy. *International Journal of Heat and Mass Transfer* 2013; 57:582–94.
- [9] Mahian O, Kianifar A, Kleinstreuer C, Al-Nimr MA, Pop I, Sahin AZ, et al. A review of entropy generation in nanofluid flow. *International Journal of Heat and Mass Transfer* 2013; 65:514–32.
- [10] Sabaghan A, Edalatpour M, Charjouei Moghadam M, Roohi E, Niazmand H. Nanofluid flow and heat transfer in a microchannel with longitudinal vortex generators: Two-phase numerical simulation. *Applied Thermal Engineering* 2016; 100:179–189.
- [11] Xuan Y, Li Q, Hu W. Aggregation structure and thermal conductivity of nanofluids. *AIChE Journal* 2003; 49(4):1038–43.

- [12] Nieto de Castro CA, Li SFY, Nagashima A, Trengove RD, Wakeham A. Standard reference data for the thermal conductivity of liquids. *Journal of Physical and Chemical Reference Data* 1986; 15:1073–86.
- [13] Corcione M. Empirical correlating equations for predicting the effective thermal conductivity and dynamic viscosity of nanofluids. *Energy Conversion and Management* 2011; 52:789–93.
- [14] Edalatpour M, Kianifar A, Aryana K, Tiwari G.N, Energy, exergy, and cost analyses of a double-glazed solar air heater using phase change material. *Journal of Renewable and Sustainable Energy* 2016; 8: 015101.
- [15] Kalogirou SA. *Solar energy engineering: processes and systems*. 2nd edition. Oxford: Elsevier; 2013.
- [16] Gnielinski V. New equations for heat and mass transfer in turbulent pipe and channel flow. *International Chemical Engineering* 1976; 16:359–68.
- [17] Colebrook CF. Turbulent flow in pipes, with particular reference to the transition region between smooth and rough pipe laws. *Journal of Institution of Civil Engineers* 1939; 11:133–56.
- [18] Çengel YA, Cimbala JM. *Fluid mechanics: fundamentals and applications*. 2nd edition. McGraw-Hill Higher Education; 2009.
- [19] Bejan A. *Entropy generation through heat and fluid flow*. New York: Wiley 1982.